Research Square

Preprints are preliminary reports that have not undergone peer review.
They should not be considered conclusive, used to inform clinical practice,
or referenced by the media as validated information.

Three-Dimensional Optical Vortices in Nonlinear Bessel Waveguides

Carlos Felipe Sánchez
Politecnica Salesiana University
Humberto Michinel
Universidade de Vigo
Boris Malomed
Tel Aviv University
Ángel Paredes
Universidade de Vigo
José Ramón Salgueiro
jrs@uvigo.es

Universidade de Vigo

Research Article

Keywords: nonlinear waves, spatio-temporal solitons, vortices, waveguides

Posted Date: March 13th, 2026

DOI: https://doi.org/10.21203/rs.3.rs-9042566/v1

License: This work is licensed under a Creative Commons Attribution 4.0 International License.
Read Full License

Additional Declarations: No competing interests reported.

Version of Record: A version of this preprint was published at Optical and Quantum Electronics on September 4th, 2026. See the published version at https://doi.org/10.1007/s11082-026-09120-8.

Three-Dimensional Optical Vortices in Nonlinear Bessel Waveguides

Carlos F. Sánchez[1,2], Humberto Michinel[2], Boris Malomed[3,4], Ángel Paredes[2], José R. Salgueiro[2*]

[1]Grupo de Investigación en Física (GIF), Universidad Politécnica Salesiana, Cuenca, 010105, Ecuador.
[2]Instituto de Física, Computación e Ciencia Aeroespacial (IFCAE), Universidade de Vigo, Campus As Lagoas, Ourense, 32004, Spain.
[3]Department of Physical Electronics, School of Electric and Computer Engineering, Faculty of Engineering, Tel Aviv University, Tel Aviv, Israel.
[4]Instituto de Alta Investigación, Universidad de Tarapacá, Casilla 7D, Arica, Chile.

*Corresponding author(s). E-mail(s): jrs@uvigo.es;

Abstract

We explore the formation, stability, and propagation dynamics of light bullets carrying orbital angular momentum (vorticity) in Bessel-structured nonlinear graded-index waveguides. While these waves are prone to the collapse in uniform three-dimensional media, we demonstrate that their stabilization is provided by a squared-Bessel index profile in the plane orthogonal to the propagation direction, which may play the role of the waveguiding or antiwaveguiding potential. We analyze the propagation dynamics in a wide experimentally accessible parameter range. Our results contribute to the understanding of nonlinear light localization in multidimensional settings and suggest new possibilities for using structured light in advanced photonic applications.

Keywords: nonlinear waves, spatio-temporal solitons, vortices, waveguides

1 Introduction

Spatiotemporal optical solitons (Malomed et al. 2005), often referred to as light bullets (LBs) (Silberberg 1990), are photonic wave packets that maintain their self-trapped shape due to the synergetic balance between diffraction, group-velocity dispersion (GVD), and optical nonlinearity. Their propagation is modeled by multidimensional nonlinear Schrödinger equations (NLSEs) (Fibich 2015), which apply to light pulses and beams in optical communications, lasers, extreme optics, and other fields (Kivshar and Agrawal 2003).

It is well known that LBs are unstable to the spontaneous onset of the catastrophic collapse (blowup) in self–focusing media with anomalous GVD (Bespalov and Talanov 1966; Sulem and Sulem 2007; Edmundson 1997). To prevent the blowup and secure stable propagation of nonlinear optical pulses in two or three spatial dimensions (2D or 3D), various mechanisms have been explored (Malomed 2022), including, *inter alia*, the incorporation of higher–order terms in the refractive index, such as saturable (Akhmediev et al. 1992; Edmundson and Enns 1992) or cubic–quintic nonlinearities (Michinel et al. 2002, 2006), as well as nonlocality (Krolikowski et al. 2001; Bang et al. 2002; Mihalache et al. 2006; Paredes et al. 2020) and appropriate potential structures (Baizakov et al. 2003; Yu et al. 1995; Mihalache et al. 2004; Raghavan and Agrawal 2000). In particular, LBs can be stabilized by means of the effective trapping provided by waveguiding linear-index profiles (Mihalache et al. 2005; Diebel et al. 2016; Aközbek and John 1998).

Further, imparting the optical angular momentum (OAM) to the self-trapped optical pulses (Nye and Berry 1974; Coullet et al. 1989) leads to the formation of vortex bullets (Desyatnikov et al. 2005,?), whose intrinsic structure is characterized by the topological charge, alias winding number (Quiroga-Teixeiro and Michinel 1997; Michinel et al. 2004; Salamin 2018). Despite their theoretical appeal and promising properties, the experimental realization of stable LBs, and especially of vortex bullets, is a highly challenging problem (Hang and Huang 2013). Control over the input beam and securing a necessary balance between competing factors are critical for achieving the sustained propagation of LBs and, more generally speaking, multidimensional solitons (Porras 2019; Chen et al. 1997; Zhang et al. 2022; Malomed 2022).

In the present paper, we explore the use of Bessel–lattice refractive–index structures in the plane transverse to the propagation direction (Mihalache et al. 2005) as a means to maintain the existence and stability of vortex bullets, cf. Refs. (Kartashov et al. 2005, 2004). For a Gaussian profile, the existence of stable spatiotemporal vortex solitons was recently demonstrated in the context of Bose-Einstein condensates (Sánchez et al. 2025), which are modeled by a variety of NLSEs in the form of Gross-Pitaevskii equations (GPEs) (Pitaevskii and Stringari 2003). We analyze the stability of the predicted self-trapped vortex modes by dint of the Vakhitov–Kolokolov (VK) stability criterion (Vakhitov and Kolokolov 1973; Fibich 2015) and systematic simulations of their propagation. Earlier, a particular case was considered (Zhong et al. 2010) with the external potential and propagation constant specifically chosen so that, under the Hartree approximation space-time factorization), the spatial radial structure of the solution reduced to the Bessel functions, while the temporal profile took the form of a hyperbolic secant. In this work, we search for general families of solutions by

addressing, in particular, the difference between the Bessel and Gaussian waveguiding structures in axially symmetric self–focusing optical media with anomalous GVD.

In the following section we introduce the theoretical framework and basic equations of the model. In section 3 we outline the numerical scheme used in this work to produce stable vortex bullets. In section 4 we present numerically generated solution families, and in section 5 we analyze their stability. The paper is concluded by section 5.

2 The model

Our starting point is the NLSE for the medium with the Kerr nonlinearity and an axially–symmetric pattern of the linear refractive index $V(r)$,

$$i\frac{\partial\Psi}{\partial z} + \nabla_\perp^2\Psi - \sigma\frac{\partial^2\Psi}{\partial T^2} + \left[V(r) + \alpha|\Psi|^2\right]\Psi = 0. \tag{1}$$

This equation governs the propagation along the the z–direction of the envelope $\Psi(r,\phi,z,T)$ of a pulsed beam. The cylindrical coordinates (r,ϕ,z) are scaled by the vacuum wavenumber $k_0 = \omega/c$, and $T = t - z/v_g$ is the reduced time, where t is the conventional time and v_g is the group velocity of the carrier wave. Other parameters are the carrier frequency ω, vacuum speed of light c, the normalized GVD coefficient $\sigma = \pm 1$, and the Kerr coefficient, which is also normalized to be $\alpha = 1$ (we consider only the self-focusing sign of the nonlinearity). Further, the transverse Laplacian $\nabla_\perp \equiv \partial_r^2 + (1/r)\partial_r + \partial_\phi^2$ represents the paraxial–diffraction operator, and the spatial pattern of the axially symmetric linear refractive index with strength $|\gamma|$ is defined as

$$V(r) = \gamma\left[F(r)\right]^2. \tag{2}$$

This definition implies that, in the experimentally relevant setup, based on the photorefractive material (Efremidis et al. 2002), the real function $F(r)$ represents the transverse structure of the ordinary-polarization optical field illuminating the waveguide. Through the XPM effect, $F(r)$ induces the effective potential, $\gamma\left[F(r)\right]^2$, guiding the probe beam launched in the extraordinary polarization. Here, we consider two different transverse structures, *viz.*, the Gaussian, with

$$F(r) = \exp(-r^2/4), \tag{3}$$

and the Bessel function,

$$F(r) = J_0(r). \tag{4}$$

In the case of the normal GVD, i.e., $\sigma = 1$ in Eq. (1), there are no solutions in the form of LBs. In this case, optical pulses do not collapse but split, instead, after a transitional compression stage. Note that another species of partly localized waves, previously known in the linear context, can also be produced by the NLSE with the self-focusing nonlinearity, *viz.*, the X-waves (Saari and Reivelt 1997) and X-solitons (Conti et al. 2003) (so called due to their characteristic shape), which were also found for focusing nonlinearities.

In the case of the anomalous GVD, $\sigma = -1$, the temporal dimension can be treated as an additional coordinate, as the full Laplacian in Eq. (1) is the sign-definite elliptical

operator. This fact makes it possible to produce fully localized spatiotemporal modes in the presence of the self-focusing nonlinear response.

In the two-dimensional case (one transverse spatial dimension plus the temporal one) there is a critical energy threshold above which the LB initiates the collapse after passing a certain distance that depends on the initial conditions, hence this collapse scenario is called a critical one. In particular, the pre-collapse distance may be significantly increased by imparting a negative chirp onto the input. If the initial energy falls below the critical value, the input decays without starting the collapse. On the other hand, in 3D (with the two transverse dimensions) the collapse is supercritical, which means that the critical energy level is zero (in other words, the input with an arbitrarily small energy may initiate the 3D collapse) (Fibich 2015; Sulem and Sulem 2007; Zakharov and Kuznetsov 2012).

In the present work, we consider the case of the self-focusing ($\alpha = 1$) in the anomalous-GVD regime, $\sigma = -1$, aiming to obtain vortex-bullet stationary solutions, introduced as

$$\Psi(r, \phi, z, T) = \psi(r, T) e^{i\ell\phi} e^{i(\beta z - \omega t)}, \tag{5}$$

where ψ is a real function, β is a real propagation constant, and ℓ is the integer vorticity, alias the topological charge. We focus on fundamental vortices, with $\ell = 1$. For a given value of β the solution is uniquely determined by its total energy, i.e., in the scaled units, the 3D norm N of the wavefunction (5), which is defined by Eq. (8) below.

3 Numerical solutions

Substituting ansatz (5) in Eq. (1), one arrives at the eigenvalue problem based on the following equation for the real field $\psi(r, T)$:

$$-\beta\psi + \frac{\partial^2\psi}{\partial T^2} + \frac{\partial^2\psi}{\partial r^2} + \frac{1}{r}\frac{\partial\psi}{\partial r} - \frac{\ell^2}{r^2}\psi + [V(r) + \psi^2]\psi = 0. \tag{6}$$

This equation was solved numerically applying the finite-differences scheme (for variables r and T) and solving iteratively the resulting nonlinear algebraic problem (Salgueiro et al. 2007). The presence of the first derivative in Eq. (6) breaks the symmetry of the linear equation system to be solved as a part of each Newton's iteration. Because solvers intended for nonsymmetric matrices are much less efficient than those for symmetric ones, we apply the known transformation $\psi(r) = r^{-1/2}u(r)$, which eliminates the first radial derivative, leading to the following equation:

$$\frac{\partial^2 u}{\partial T^2} + \frac{\partial^2 u}{\partial r^2} - \frac{(\ell^2 - 1/4)}{r^2}u + \left[V(r) - \beta + \frac{u^2}{r}\right] u = 0, \tag{7}$$

with the 3D norm

$$N = 2\pi \int_{-\infty}^{+\infty} \int_0^{\infty} |\psi|^2 r dr\, dT = 2\pi \int_{-\infty}^{+\infty} \int_0^{\infty} |u|^2 dr\, dT. \tag{8}$$

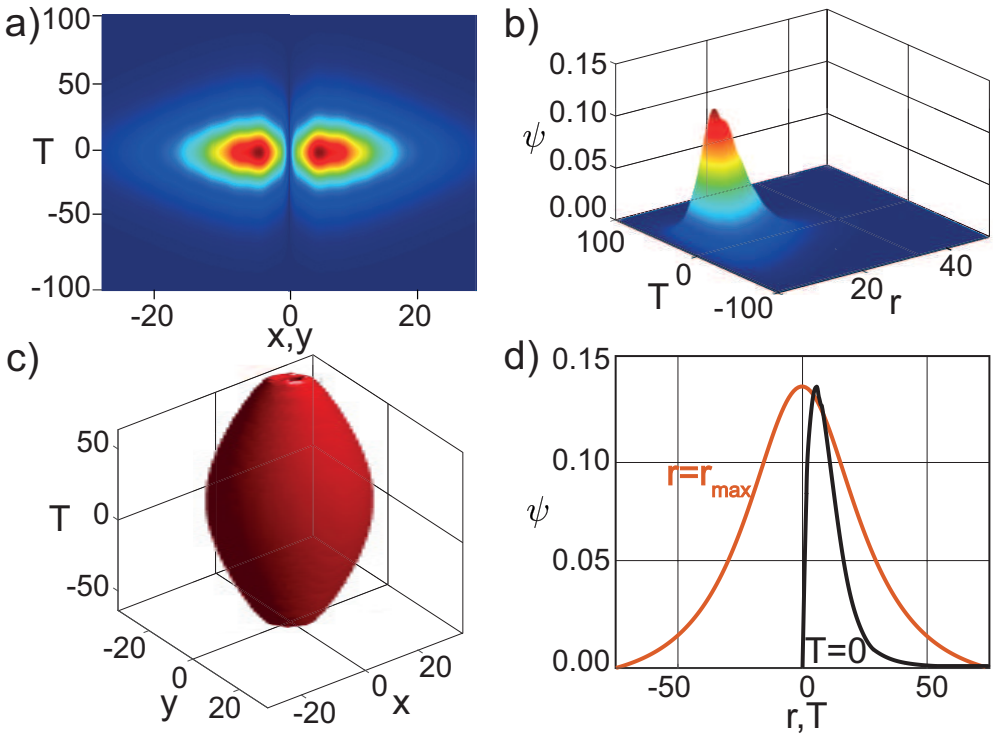


Fig. 1 An example of the numerical solution of Eq. (6) for the Bessel lattice defined as per Eqs. (2) and (4), with $\ell = 1$, $\gamma = 2$ and $\beta = 0.05$. Shown are views of the contour in (a) and mesh in (b) of the field in the plane (r, T), and the 3D isosurface view in (c). Panel (d): the spatial and temporal profiles, plotted in cross-sections $T = 0$ and $r = r_{\max}$, where $r_{\max}$ is the radial coordinate corresponding to the maximum of $|\psi|$.

Solutions to Eq. (7) must satisfy the boundary condition $u(r = 0) = 0$, hence producing a regular solution for $\psi(r)$ at $r \to 0$ in spite of the diverging factor $r^{-1/2}$ in the above transformation.

Examples of numerically found solutions are displayed in Figs. 1 and 2 for the waveguide with the squared-Bessel potential profile defined as per Eqs. (2) and (4). The vortex structure, with the cylindrical symmetry, demonstrates itself in the spatial transversal plane (x, y) [alias (r, ϕ), in the polar coordinates]. Thus, the stationary states can be adequately represented in terms of the spatial and temporal coordinates, r and T.

In Fig. 3 we additionally plot several radial and temporal profiles of the stationary states for the propagation constant $\beta = 0.25$, corresponding to two different waveguides with strength $\gamma = 2$ (a-b) and $\gamma = 4$ (c-d). Solid lines are the modal profiles obtained for the squared-Bessel waveguiding structure, indicated by the shadowed area in the plots, and the dashed curves correspond to the Gaussian structure defined as per Eqs. (2) and (3). Both structures are chosen so as to have the same width.

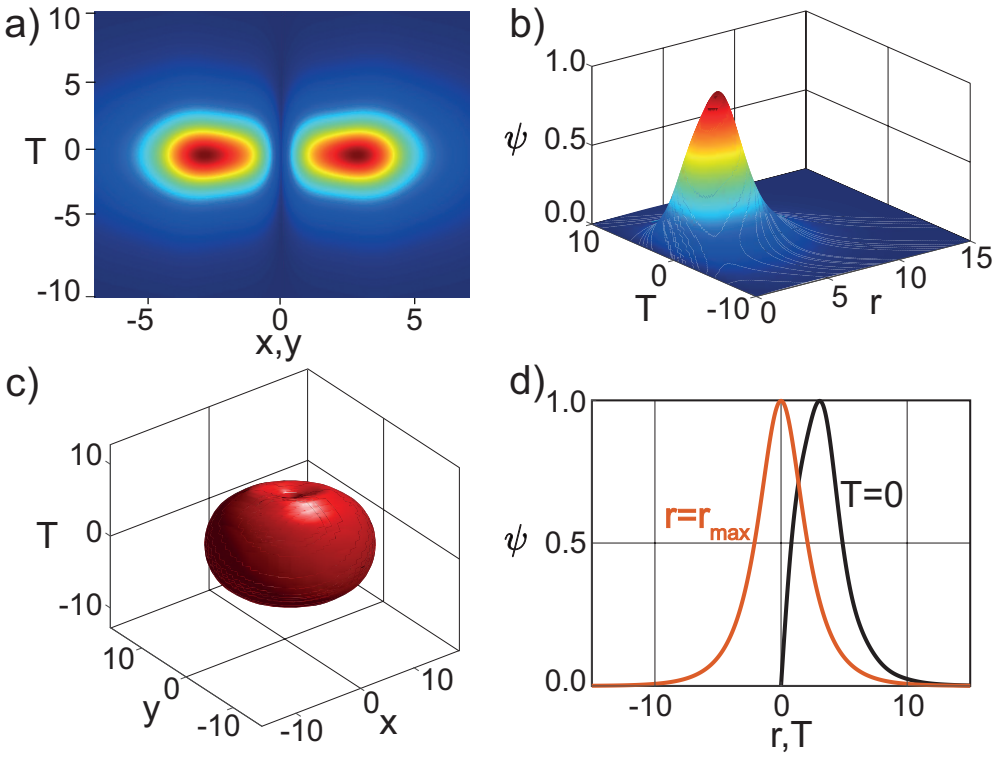


Fig. 2 The same as Fig. 1, but for $\gamma = 2$, $\ell = 1$ and $\beta = 0.25$.

As it can be seen in the plots, for $\gamma = 2$ and propagation constant $\beta = 0.25$, there is only one stationary state or three different ones, maintained by the Gaussian or Bessel waveguides respectively. This is due to the fact that the $J_0^2(r)$ function has adjacent maxima that can dramatically change the guiding properties of the system through the interplay with the self-focusing nonlinearity. For $\gamma = 4$ (deeper waveguides) there is a single stationary state with $\beta = 0.25$, in the Gaussian and Bessel waveguides alike. Naturally, the profiles with higher energy (larger values of norm N) are more focused in the temporal dimension, as seen in the right-column plots of Fig. 3. Note also that, for deeper waveguides [larger γ in Eq. (2)], smaller energy is required to induce the nonlinear self-trapping. Accordingly, positions of maxima of the stationary states in stronger waveguides are closer to local maxima of the refractive index.

Figure 4 is similar to Fig. 3 but for the *antiwaveguides* (AWGs) (Gisin and Hardy 1995; Bortman-Arbiv et al. 2001; Kaplan et al. 2002), with $\gamma = -2$ or $\gamma = -4$ (the top and bottom rows respectively) and $\beta = 0.25$. Due to the self–focusing effect, stationary LBs can be found in this case too. As in the case presented in Fig. 3, there are several eigenstates with the same value of β for the Bessel AWG and a single one for the anti-Gaussian. Notably, both for the lower ($\gamma = -2$) and higher ($\gamma = -4$) Bessel AWGs, three LBs with different radial profiles are found. Note that the temporal shapes of

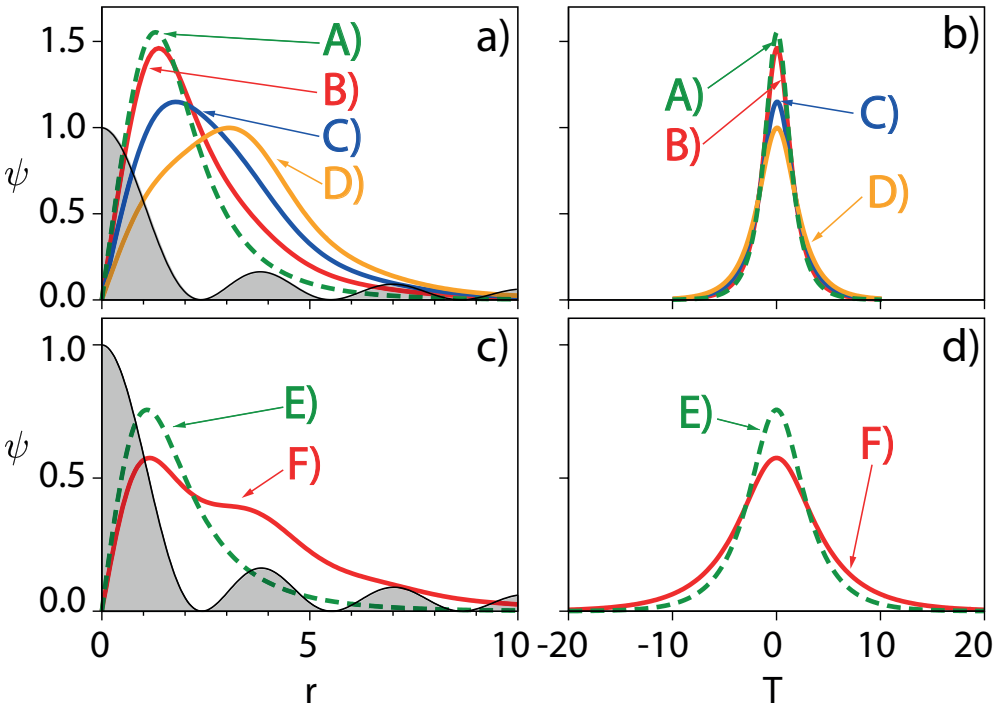


Fig. 3 Examples of the numerically calculated profiles of the vortex bullets along r and T (the left and right panels, respectively) for $\beta = 0.25$ and $\gamma = 2$ in (a,b), and $\gamma = 4$ in (c,d). The thin line bounding the shadowed area is the normalized squared-Bessel profile, $J_0^2(r)$. The colored solid and dashed curves correspond, severally, to the Bessel and Gaussian waveguiding structures. The profiles labelled with letters correspond to the white dots in Figs. 6 and 8 marked with the same labels.

the LBs are nearly identical for close values of the energy (N), as the temporal shape is not directly affected by the transverse (anti)waveguiding structure.

In Fig. 4 the situation for the Gaussian AWG agrees with what might be expected: for the stronger AWG structure (larger $-\gamma$), more energy is necessary to achieve the self-trapping, the maxima being located at almost the same position for $\gamma = -2$ and $\gamma = -4$. On the other hand, in the case of the Bessel AWG with its set of local potential minima, a more complex interplay with the self-focusing is observed. For instance, comparing two red profiles in the left-column panels, one can see that the trapping may occur around the same position, with less energy for the higher AWG structure, which might not be expected in the absence of the local potential minima (as in the Gaussian case).

Figure 5 is similar to Fig. 4 but for $\beta = 1.6$, with the top and bottom panels corresponding to $\gamma = -2$ and $\gamma = -4$, respectively. Contrary to Fig. 4, Fig. 5 demonstrates several eigenstates with the same value of β, both for the Bessel and Gaussian AWGs

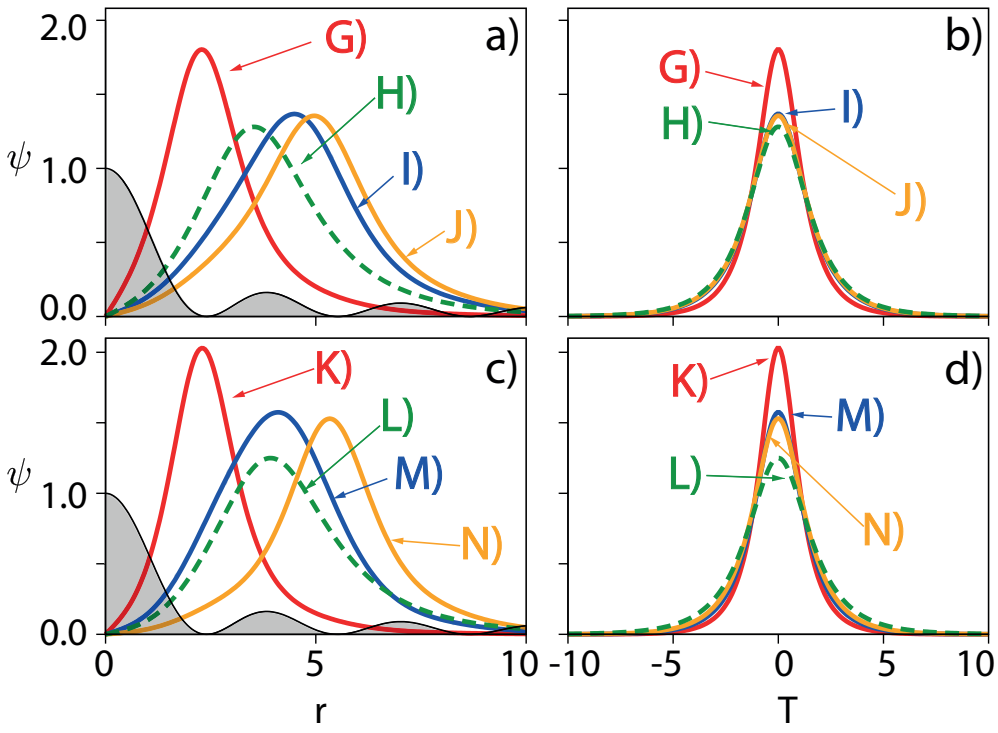


Fig. 4 The same as in Fig. 3, but for the AWG, with $\gamma < 0$ and $\beta = 0.2$. Top and bottom panels correspond to $\gamma = -2$ and $\gamma = -4$ respectively. The profiles labelled with letters correspond to the white dots marked with the same labels in Figs. 7 and 8.

with $\gamma = -4$. On the other hand, for the weaker AWG with $\gamma = -2$, a single stationary state with $\beta = 1.6$ is found for the Gaussian and Bessel structures alike. As above, the temporal distributions are nearly identical for close values of the pulse energy. It is also seen that both the radial and temporal profiles are quite similar for the Bessel and Gaussian structure, which is not surprising as the self-trapping is chiefly determined by the nonlinearity.

4 Solution families

To gain insight into the physical properties of the LB stationary states, we classify them into families parametrized by the values of their propagation constant and energy (i.e., norm N). In Fig. 6 we present the families for the guiding profile ($\gamma > 0$), by means of $N(\beta)$ curves, for $\gamma = 2$ and $\gamma = 4$. The case of $\gamma = 0$ corresponds to the

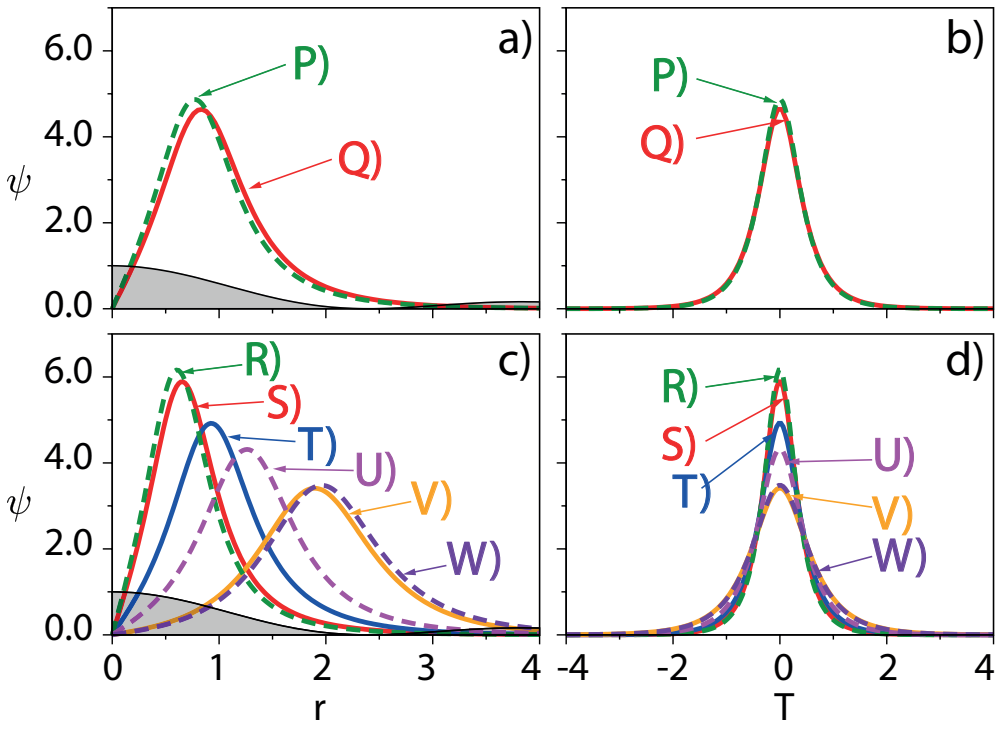


Fig. 5 The same as in Fig. 4, but for $\beta = 1.6$. The top and bottom panels correspond to $\gamma = -2$ and $\gamma = -4$, respectively. The profiles labelled with letters correspond to the white dots marked with the same labels in Figs. 7 and 8.

uniform Kerr medium, and is also shown in the plot. The continuous and dashed curves correspond, respectively, to the LBs maintained by the squared-Bessel and Gaussian waveguiding structures. The inset displays both index profiles. A filled dot indicates the stationary solution from Fig. 1, and a vertical gray line at $\beta = 0.25$ cuts the curves at empty white spots that correspond to the stationary solutions shown in Fig. 3.

As seen in Fig. 6, in the absence of the waveguiding structure ($\gamma = 0$) the norm diverges at $\beta \to 0$, while it is well known that no stable solutions exist in this case (Fibich 2015; Malomed 2022). The presence of the waveguiding structure ($\gamma > 0$) dramatically changes the behavior, generating a cutoff value for the propagation constant in the linear limit ($N = 0$), which corresponds to the guiding supported exclusively by the refractive-index distribution. As shown by the solid curves with $\gamma = 2$ and $\gamma = 4$, the energy initially grows with β, attaining a maximum and subsequently decreasing. The strength threshold to observe this cutoff is lower for the squared-Bessel profile than for the Gaussian one as is evident from the dashed curve correspondent to $\gamma = 2$, which does not shown either the cutoff point or the initial raising energy. We again stress that multiple states with the same value of the propagation constant β can be maintained by the Bessel structure with $\gamma = 2$, as it was mentioned above, in the relation to Fig. 3.

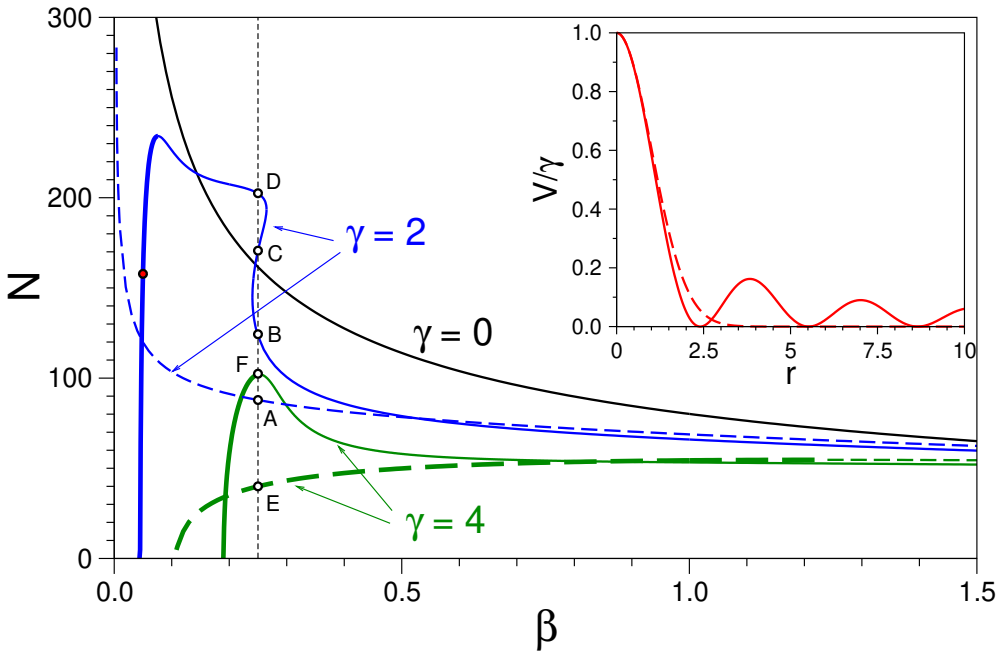


Fig. 6 Norm N of several families of stationary LB solutions vs. the propagation constant β for the values of the waveguide strength $\gamma = 0$, 2, and 4. Continuous and dashed curves correspond, respectively, to the LBs maintained by the Bessel and Gaussian waveguiding structures. Thicker sections of the curves indicate the domain where LBs are stable. The black curve with $\gamma = 0$ is included for the comparison. White empty dots correspond to the LB profiles of the same label plotted in Fig. 3. The filled dot indicates the stable LB in Fig. 1. The inset shows the respective waveguiding profiles, *viz.*, the squared-Bessel and Gaussian ones (continuous and dashed curve, respectively).

In Fig. 7 we show the families for the AWG profile ($\gamma < 0$). In this case, N may increase indefinitely with decreasing values of β. Also, valid values of β, i.e. those leading to bounded modes, may now be negative due to the AWG potential. As the potential strength, $-\gamma$, increases, there appears S-shaped features on the $N(\beta)$ curve, which is demonstrated by Fig. 7 for $\beta = -4$ in the interval of, roughly speaking, $1.5 < \beta < 2.3$. On the other hand, at large values of N ($N \sim 350$) the same figure demonstrates a prolate loop, detached from the main curve. Large values of ring radius of the corresponding states suggest that they are related to the first maximum of the respective Bessel potential.

In Fig. 8 we plot the norm N vs. strength γ of the squared-Bessel potential for different values of the propagation constant, β. The plot helps to identify intervals of γ where multiple stationary solutions exist. They feature a loop shape – for instance, the loop for $\beta = 0.25$ in the interval $1.22 < \gamma < 2.84$, where three different stationary solutions are found. At particular values of γ the loop self-crosses, as it happens for $\beta = 0.20$, close to $\gamma = -4$ (in the case of the AWG structure), implying the detachment of the loop from the main curve. For a particular value of β, the curve attains $N = 0$ (e.g., at $\gamma \approx 8.5$ for $\gamma = 1.60$ in Fig. 8) which implies reaching the limit where

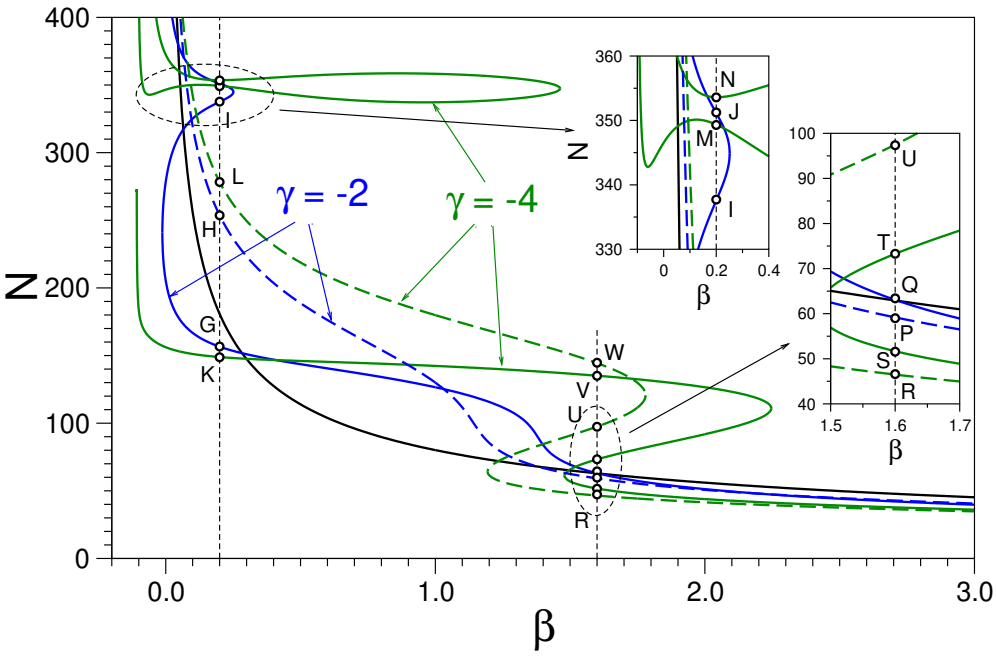


Fig. 7 The same as Fig. 6 for different values $\gamma < 0$ of the AWG strength parameter. White dots labelled with letters correspond to the LB profiles of the same label displayed in Figs. 4 and 5. Insets reproduce zoomed regions of the main plot for a better clarity.

amplitude decreases to zero as the temporal-width diverges to infinity. This happens as the nonlinearity is no longer able to keep the state bounded in the temporal direction, although the potential, if it is strong enough, would confine the state in the spatial one.

5 The stability analysis

5.1 The Vakhitov-Kolokolov (VK) criterion

The stability of the stationary solutions can be assessed, in the quasi-analytical form, by means of the VK criterion which states that a necessary condition for the stability of a stationary solution, taken as per Eq. (5), is $dN/d\beta > 0$ (Vakhitov and Kolokolov 1973; Fibich 2015). Conversely, the solution is definitely unstable in the case of $dN/d\beta < 0$. The VK criterion actually implies the absence of unstable eigenmodes of small perturbations with purely real instability growth rates. Note that the ubiquitous instability of vortex solitons against spontaneous splitting into fragments is not detected by the VK criterion because the splitting instability is accounted by complex growth rates. Eventually, numerical simulation of the propagation should verify which stationary states are truly stable.

In the free-space case, with $\gamma = 0$, the monotonously decreasing $N(\beta)$ dependence in Fig. 6 predicts, as expected, the fully unstable LB family. Analyzing the other curves in Fig. 6 with respect to the VK criterion we arrive at the following conclusions:

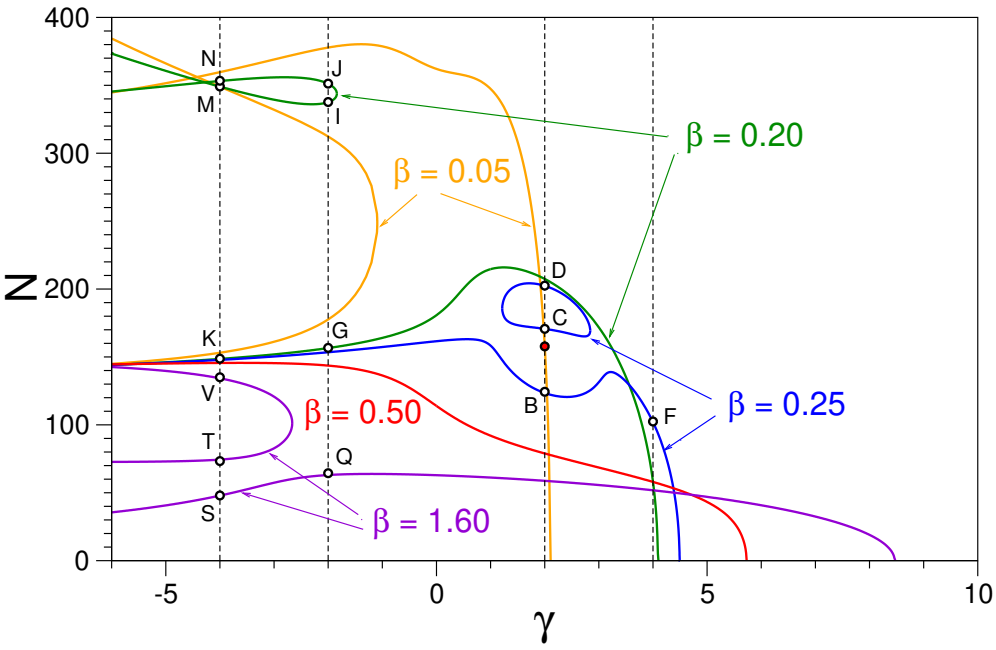


Fig. 8 The norm N of the stationary LB vs. the Bessel-potential strength γ, for different fixed values of the propagation constant β. The red dot indicates the stable state shown in Fig. 1. White dots with labels correspond to the profiles with the same label displayed in Figs. 3, 4 and 5.

- For $\gamma = 2$, the dashed curve for the Gaussian potential remains monotonically decreasing, which means the full instability.
- For $\gamma = 4$, the green dashed curve for the Gaussian potential monotonously increases at $\beta < 1.24$, attaining a maximum, and decreases at $\beta > 1.24$. Hence stable stationary states may be possible at $\beta < 1.24$. These possibilities for the Gaussian trapping potential have been analyzed in Ref. (Sánchez et al. 2025) in the context of Bose-Einstein condensates and it was concluded they were fully stable.
- For $\gamma = 2$ with the squared-Bessel potential the situation is more complex, suggesting regions of multi-stability and alternating stable and unstable fragments with stationary solutions having the same value of the propagation constant, corresponding to different values of norm N, around the region with $\beta = 0.25$.
- For $\gamma = 4$ with the squared-Bessel potential the situation is qualitatively similar to that for the Gaussian potential, with the value of $\beta = 0.26$ marking the transition from stable to unstable solutions.

The physical implication of these observations is that the effective Bessel potential introduces a rich stability/instability pattern and the corresponding bifurcation structure. Indeed, the $N(\beta)$ curves exhibit loops and turning points, reflecting the impact of the potential on the existence and stability of the LBs. The conclusion is that, while low–energy solutions may be stabilized by the potential, the stability is maintained in specific intervals of β.

With respect to Fig. 7, that corresponds to the AWG potential with $\gamma < 0$, the conclusions are:

- For $\gamma = -2$, the dashed curve for the Gaussian potential is monotonically decreasing, indicating the full instability in this case.
- For $\gamma = -4$, the dashed curve for the Gaussian case displays a Z-like shape in the interval of $1.2 < \beta < 1.8$, which is compatible with possible bistability.
- For $\gamma = -2$ with the squared-Bessel potential (the continuous curve), three stationary states with different values of the norm exist in the interval of $0 < \beta < 0.25$, and only a single state at $\beta > 0.25$. According to the VK criterion, stable states may exist for increasing $N(\beta)$ branches.
- For $\gamma = -4$ with the squared-Bessel potential (the continuous line), the situation is still more complex, due to conspicuous oscillations of the $N(\beta)$ curve, indicating possible multi-stability windows, that should be explored by means of numerical simulations.

To conclude, stationary states which are potentially stable according to the VK criterion may exist both for the waveguiding and AWG potentials, for both the squared-Gaussian and Bessel potentials. The depth of the waveguide plays a crucial role in predicting the VK-stability regions.

5.2 Numerical simulations.

To finally verify the stability of the stationary LBs, we used the standard beam-propagation method, based on the finite-difference discretization of Eq. (1). The results are reported in Figs. 9-11.

As concerns the LBs in the guiding-type potential ($\gamma > 0$), we have found that they are indeed stable in the region of $\partial N/\partial\beta > 0$, as predicted by the VK criterion. We have checked this conclusion by means of the long-distance propagation, up to $z = 500$.

We also simulated collisions between LBs, as shown in Fig. 9, which demonstrate that such collisions are quasi-elastic. In this case, the colliding LBs are out of phase, so that they bounce back after the collision. In case both LBs are in phase they temporary mix to subsequently emerge after crossing themselves.

In the direct simulations the VK-unstable LBs, belonging to the region of $dN/d\beta < 0$, collapse to a small spot and then spread out. The collapsing distance is shorter for larger β, as seen in the examples shown in Fig. 10. Interestingly, the above-mentioned splitting (azimuthal) instability is not directly observed in this regime with $\gamma > 0$. It may occur only at the post-collapse stage.

In the case of an AWG potential, we observe three instability stages in the evolution: an initial azimuthal splitting (producing four fragments in most cases), followed by the collapse of the fragments into thin spikes, and then spreading of the spikes which ultimately fuse into a broadening ring. This instability scenario takes place for all values of β (see examples for $\gamma = -4$ and different values of β in Figs. 11(a-b), including those in the regions of Z-shaped $N(\beta)$ curves), revealing that in this case meeting the VK criterion does not lead to stability. In the upper loop of the curve (the one detached from the main one), see Fig. 7, the instability scenario is similar, see

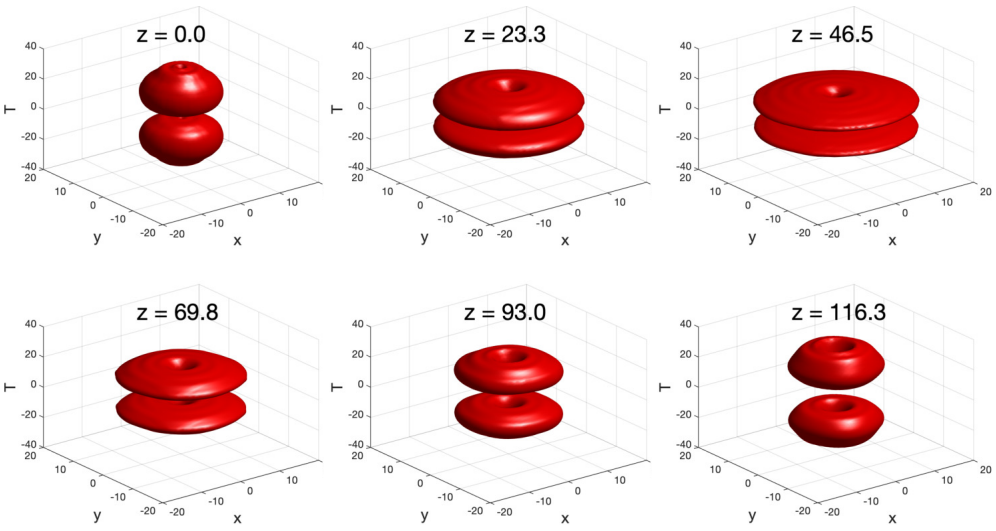


Fig. 9 An example of the elastic collision (rebound) of two stable LBs with opposite signs (the phase difference of π), for $\gamma = 4$, $\beta = 0.21$. Top row: the approach stage; bottom row: the bouncing stage.

Fig. 11(c), but at large enough values of β, where the radius of the vortex ring is larger, splitting instability produces eight fragments instead of four, as shown in Fig. 11(d).

6 Conclusion

In this work, we have studied the formation, stability, and propagation dynamics of LBs (light bullets) carrying orbital angular momentum (vorticity) in nonlinear graded-index waveguides. The analysis was performed for the fundamental vortex modes with topological charge $\ell = 1$. We have focused on two profiles of the effective potential in the plane orthogonal to the propagation direction, *viz.*, the Gaussian and the squared-Bessel ones, which may be waveguiding or AWG (antiwaveguiding). Both potentials can be experimentally realized in optics, using photorefractive materials. The crucially important stability problem for the vortex LBs was tackled with the help of the VK (Vakhitov-Kolokolov) criterion; then, the stability was accurately identified by means of systematic propagation simulations. We have thus demonstrated the existence of stable vortex LBs under experimentally accessible conditions. We have also extensively analyzed the evolution of unstable LBs, which displays various dynamical phenomena.

These results contribute to the understanding of the nonlinear light localization in multidimensional systems and suggest new possibilities for controlling structured light in advanced photonic applications.

Acknowledgements. This work is a part of the R&D&i projects PID2023-146884NB-I00 funded by Ministerio de Ciencia e Innovación of Spain and GPC ED431B 2024/42 funded by Xunta de Galicia (Spain)

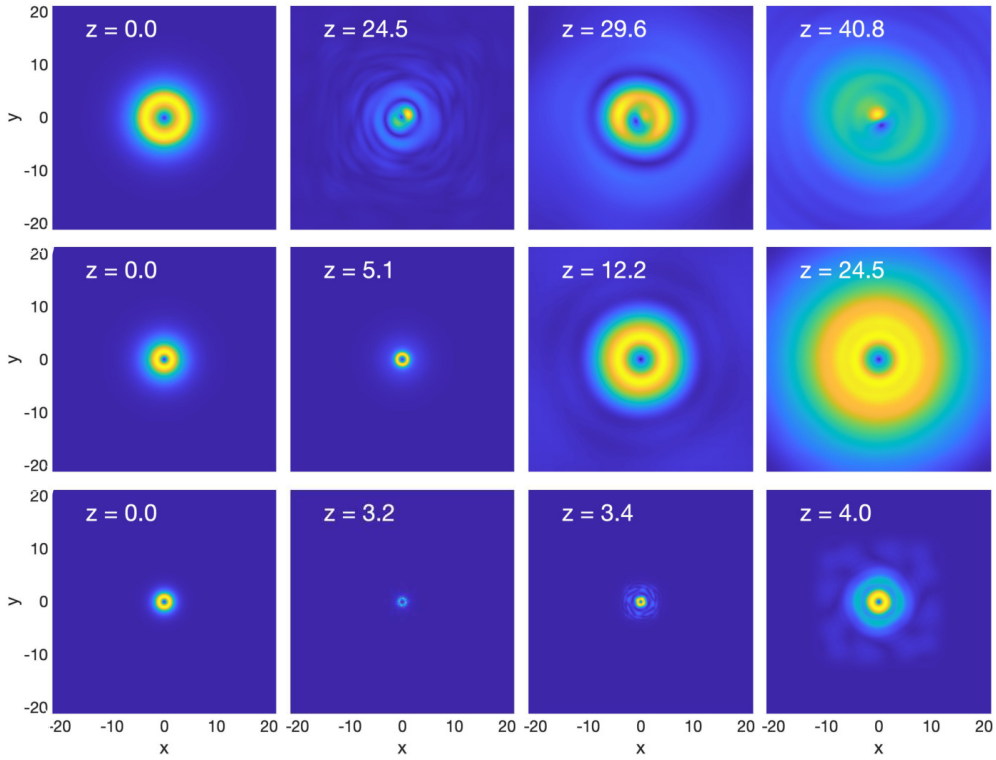


Fig. 10 Examples of the collapsing evolution of VK-unstable LBs, guided by the squared-Bessel potential with $\gamma = 2$, see Eqs. (2) and (4): (a) for $\beta = 0.2$, (b) for $\beta = 0.25$, (c) for $\beta = 1.0$.

Declarations

- Funding. This research was supported by projects PID2023-146884NB-I00 of Ministerio de Ciencia e Innovación of Spain and GPC ED431B 2024/42 of Xunta de Galicia (Spain)
- Conflict of interest/Competing interests. The authors have no relevant financial or non-financial interests to disclose.
- Data availability. The datasets generated during the current study and selected to compose the different figures in the manuscript are available in https://doi.org/10.5281/zenodo.18861294
- Author contribution. All authors contributed to the research conception and preparation of this manuscript and have approved the final version.

References

Aközbek, N., John, S.: Optical solitary waves in two-and three-dimensional nonlinear photonic band-gap structures. Physical Review E **57**(2), 2287 (1998)

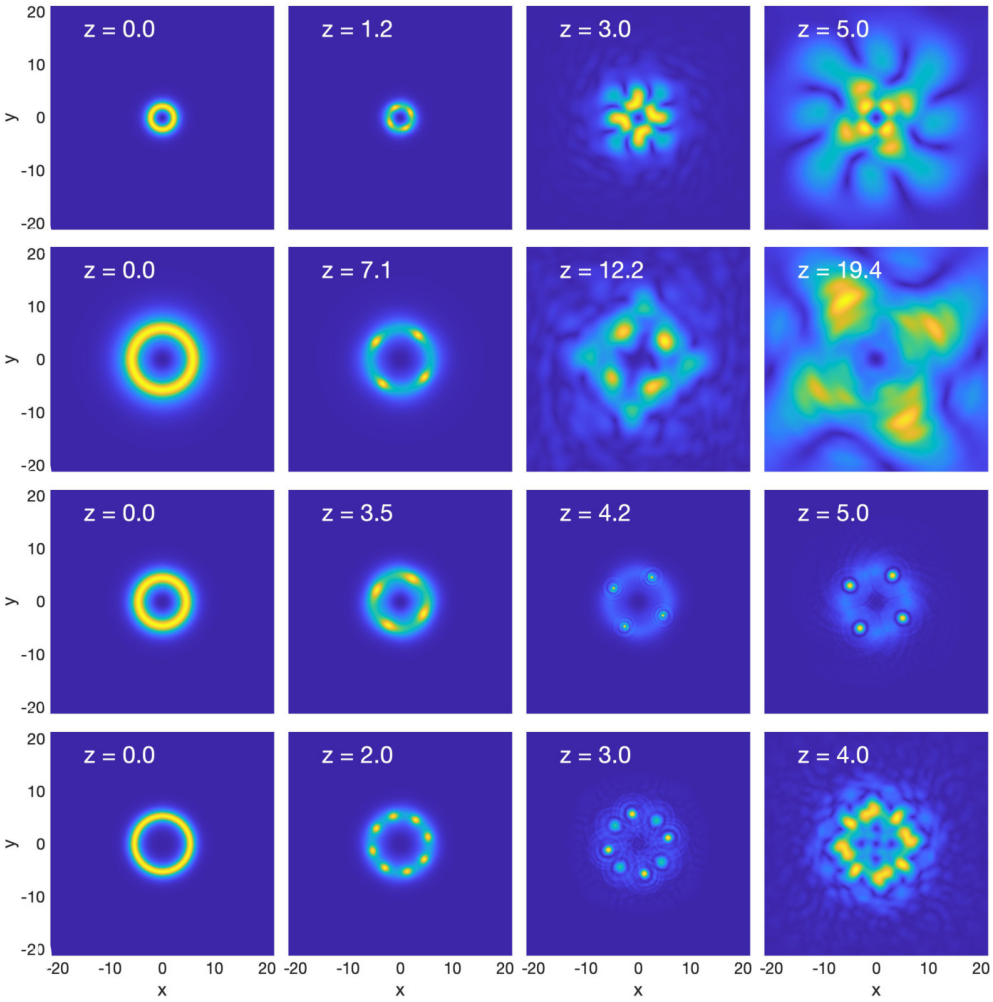


Fig. 11 Instability scenarios of different LBs for the AWG squared-Bessel-like potential, with $\gamma = -4$. (a) $\beta = 1.0$, (b) $\beta = 0.05$, (c) $\beta = 0.5$ (this case belongs to the loop of the $N(\beta)$ curve, see Fig. 7), (d) $\beta = 1.2$ (this case also belongs to the loop).

Akhmediev, N.N., Korneev, V., Nabiev, R.F.: Modulation instability of the ground state of the nonlinear wave equation: optical machine gun. Optics letters **17**(6), 393–395 (1992)

Bortman-Arbiv, D., Wilson-Gordon, A.D., Friedmann, H.: Strong parametric amplification by spatial soliton-induced cloning of transverse beam profiles in an all-optical antiwaveguide. Phys. Rev. A **63**, 031801 (2001) https://doi.org/10.1103/PhysRevA.63.031801

Bang, O., Krolikowski, W., Wyller, J., Rasmussen, J.J.: Collapse arrest and soliton

stabilization in nonlocal nonlinear media. Physical Review E **66**(4), 046619 (2002)

Baizakov, B.B., Malomed, B.A., Salerno, M.: Multidimensional solitons in periodic potentials. Europhysics letters **63**(5), 642 (2003)

Bespalov, V.I., Talanov, V.I.: Filamentary structure of light beams in nonlinear liquids. Soviet Journal of Experimental and Theoretical Physics Letters **3**, 307 (1966)

Coullet, P., Gil, L., Rocca, F.: Optical vortices. Optics Communications **73**(5), 403–408 (1989)

Chen, Z., Segev, M., Wilson, D.W., Muller, R.E., Maker, P.D.: Self-trapping of an optical vortex by use of the bulk photovoltaic effect. Physical Review Letters **78**(15), 2948 (1997)

Conti, C., Trillo, S., Di Trapani, P., Valiulis, G., Piskarskas, A., Jedrkiewicz, O., Trull, J.: Nonlinear electromagnetic x waves. Physical Review Letters **90**(17), 170406 (2003)

Diebel, F., Boguslawski, M., Dadalyan, T., Drampyan, R., Denz, C.: Controlled soliton formation in tailored bessel photonic lattices. Optics Express **24**(12), 12933–12940 (2016)

Desyatnikov, A.S., Kivshar, Y.S., Torner, L.: Optical vortices and vortex solitons. In: Progress in Optics vol. 47, pp. 291–391. Elsevier, (2005)

Desyatnikov, A.S., Sukhorukov, A.A., Kivshar, Y.S.: Azimuthons: spatially modulated vortex solitons. Physical review letters **95**(20), 203904 (2005)

Edmundson, D.E.: Unstable higher modes of a three-dimensional nonlinear schrödinger equation. Physical Review E **55**(6), 7636 (1997)

Edmundson, D., Enns, R.: Robust bistable light bullets. Optics Letters **17**(8), 586–588 (1992)

Efremidis, N.K., Sears, S., Christodoulides, D.N., Fleischer, J.W., Segev, M.: Discrete solitons in photorefractive optically induced photonic lattices. Phys. Rev. E **66**, 046602 (2002) https://doi.org/10.1103/PhysRevE.66.046602

Fibich, G.: The Nonlinear Schrödinger Equation: Singular Solutions and Optical Collapse. Applied Mathematical Sciences. Springer, Switzerland (2015)

Gisin, B.V., Hardy, A.A.: Stationary solutions of plane nonlinear optical antiwaveguides. Optical and Quantum Electronics **27**(6), 565–575 (1995) https://doi.org/10.1007/BF00563140

Hang, C., Huang, G.: Ultraslow helical optical bullets and their acceleration in magneto-optically controlled coherent atomic media. Physical Review A—Atomic,

Molecular, and Optical Physics **87**(5), 053809 (2013)

Kivshar, Y.S., Agrawal, G.P.: Optical Solitons: from Fibers to Photonic Crystals. Academic press, San Diego, California (2003)

Krolikowski, W., Bang, O., Rasmussen, J.J., Wyller, J.: Modulational instability in nonlocal nonlinear kerr media. Physical Review E **64**(1), 016612 (2001)

Kaplan, A., Gisin, B.V., Malomed, B.A.: Stable propagation and all-optical switching in planar waveguide–antiwaveguide periodic structures. J. Opt. Soc. Am. B **19**(3), 522–528 (2002) https://doi.org/10.1364/JOSAB.19.000522

Kartashov, Y.V., Vysloukh, V.A., Torner, L.: Rotary solitons in bessel photonic lattices. arXiv preprint physics/0407012 (2004)

Kartashov, Y.V., Vysloukh, V.A., Torner, L.: Soliton spiraling in optically induced rotating bessel lattices. Optics letters **30**(6), 637–639 (2005)

Malomed, B.A.: Multidimensional Solitons. AIP Publishing, Melville, New York (2022)

Michinel, H., Campo-Táboas, J., García-Fernández, R., Salgueiro, J., Quiroga-Teixeiro, M.: Liquid light condensates. Physical Review E **65**(6), 066604 (2002)

Mihalache, D., Mazilu, D., Lederer, F., Kartashov, Y.V., Crasovan, L.-C., Torner, L.: Stable three-dimensional spatiotemporal solitons in a two-dimensional photonic lattice. Phys. Rev. E **70**, 055603 (2004) https://doi.org/10.1103/PhysRevE.70.055603

Mihalache, D., Mazilu, D., Lederer, F., Malomed, B., Kartashov, Y.V., Crasovan, L.-C., Torner, L.: Stable spatiotemporal solitons in bessel optical lattices. Physical review letters **95**(2), 023902 (2005)

Mihalache, D., Mazilu, D., Lederer, F., Malomed, B., Kartashov, Y.V., Crasovan, L.-C., Torner, L.: Three-dimensional spatiotemporal optical solitons in nonlocal nonlinear media. Physical Review E—Statistical, Nonlinear, and Soft Matter Physics **73**(2), 025601 (2006)

Malomed, B.A., Mihalache, D., Wise, F., Torner, L.: Spatiotemporal optical solitons. Journal of Optics B: Quantum and Semiclassical Optics **7**(5), 53 (2005)

Michinel, H., Paz-Alonso, M.J., Pérez-García, V.M.: Turning light into a liquid via atomic coherence. Phys. Rev. Lett. **96**(2), 023903 (2006)

Michinel, H., Salgueiro, J.R., Paz-Alonso, M.J.: Square vortex solitons with a large angular momentum. Phys. Rev. E **70**(6), 066605 (2004)

Nye, J.F., Berry, M.V.: Dislocations in wave trains. Proc. Math. Phys. Eng. Sci.

336(1605), 165–190 (1974)

Paredes, A., Olivieri, D.N., Michinel, H.: From optics to dark matter: A review on nonlinear schrödinger–poisson systems. Physica D: Nonlinear Phenomena **403**, 132301 (2020)

Porras, M.A.: Upper bound to the orbital angular momentum carried by an ultrashort pulse. Physical Review Letters **122**(12), 123904 (2019)

Pitaevskii, L., Stringari, S.: Bose-Einstein Condensation. Oxford University Press, Oxford (2003)

Quiroga-Teixeiro, M., Michinel, H.: Stable azimuthal stationary state in quintic nonlinear optical media. J. Opt. Soc. Am. B **14**(8), 2004–2009 (1997)

Raghavan, S., Agrawal, G.P.: Spatiotemporal solitons in inhomogeneous nonlinear media. Optics Communications **180**(4), 377–382 (2000) https://doi.org/10.1016/S0030-4018(00)00727-6

Salamin, Y.I.: Fields of a bessel-bessel light bullet of arbitrary order in an under-dense plasma. Scientific Reports **8**(1), 11362 (2018)

Silberberg, Y.: Collapse of optical pulses. Optics letters **15**(22), 1282–1284 (1990)

Salgueiro, J.R., Olivieri, D., Michinel, H.: Computation of linear and nonlinear stationary states of photonic structures using modern iterative solvers. Optical and quantum electronics **39**, 239–260 (2007)

Sánchez, C.F., Paredes, Á., Michinel, H., Malomed, B.A., Salgueiro, J.R.: Guided vortex bullets. Phys. Rev. Lett., (2025) https://doi.org/10.1103/6mj1-yc1m

Saari, P., Reivelt, K.: Evidence of x-shaped propagation-invariant localized light waves. Physical Review Letters **79**(21), 4135 (1997)

Sulem, C., Sulem, P.-L.: The Nonlinear Schrödinger Equation: Self-focusing and Wave Collapse vol. 139. Springer, New York (2007)

Vakhitov, N.G., Kolokolov, A.A.: Stationary solutions of the wave equation in the medium with nonlinearity saturation. Radiophysics and Quantum Electronics **16**(7), 783–789 (1973)

Yu, S.-S., Chien, C.-H., Lai, Y., Wang, J.: Spatio-temporal solitary pulses in graded-index materials with kerr nonlinearity. Optics Communications **119**(1), 167–170 (1995) https://doi.org/10.1016/0030-4018(95)00377-K

Zhong, W.-P., Belić, M., Huang, T.: Three-dimensional bessel light bullets in self-focusing kerr media. Physical Review A—Atomic, Molecular, and Optical Physics **82**(3), 033834 (2010)

Zakharov, V.E., Kuznetsov, E.A.: Solitons and collapses: two evolution scenarios of nonlinear wave systems. Physics-Uspekhi **55**, 535–556 (2012)

Zhang, H., Zhou, T., Dai, C.: Stabilization of higher-order vortex solitons by means of nonlocal nonlinearity. Physical Review A **105**(1), 013520 (2022)